Hindawi

Research Article

Optimizing the Parameters of Spark Plasma Sintering to Enhance the Hardness of MgO/TiC Composites

Sai Ashish Kumar Karanam [ID],[1] **R. Rathinam** [ID],[2] **Pradeep Kumar Mouria,**[3] **Arnold C. Alguno,**[4] **Rey Y. Capangpangan** [ID],[5] **Tariku Achamyeleh** [ID],[6] **Jose Luis Arias Gonzales** [ID],[7] **Vijay Kumar Sharma** [ID],[8] **and T. Stephen Livingston** [ID][9]

[1]*Department of Mechanical Engineering, AU College of Engineering, Andhra University, Visakhapatnam, Andhra Pradesh, India*
[2]*Department of Chemistry, Sri Eshwar College of Engineering, Coimbatore 641202, Tamilnadu, India*
[3]*Mechanical Engineering, Manav Rachna University, Faridabad, India*
[4]*Department of Physics and Premier Research Institute of Science and Mathematics,*
 Mindanao State University—Iligan Institute of Technology, Tibanga Highway, Iligan City 9200, Philippines
[5]*Department of Physical Sciences and Mathematics, College of Marine and Allied Sciences,*
 Mindanao State University at Naawan, Poblacion, Naawan 9023, Misamis Oriental, Philippines
[6]*Mechanical Engineering, Debre Tabor University, Debra Tabor, Ethiopia*
[7]*Pontifical Catholic University of Peru, Lima, Peru*
[8]*Department of Physics, Shyam Lal College, University of Delhi, Shahdara, Delhi, India*
[9]*Department of Mechanical Engineering, Study World College of Engineering, Coimbatore, Tamilnadu, India*

Correspondence should be addressed to Tariku Achamyeleh; tariku.achamyeleh@mu.edu.et

In this research, the first work was carried out to manufacture MgO-based metal matrix composite containing 3 wt%. Sintering parameters, such as temperature, pressure, and time were subjected to Taguchi analysis to identify the most significant effect on magnesium oxide physical and mechanical characteristics. The impact of each sintering parameter explores using the analysis of variance-structure and microstructure analysis using XRD and EDS-equipped FE-SEM. The mechanical properties of the composite are evaluated by testing its Rockwell hardness (HR) and Vickers hardness (HV). The results showed that sintering temperature was the most influential of the sintering factors on microhardness. Densification at its peak was 100%, while it peaked at 62.19 Rockwell hardness and 58.7 Vickers hardness.

1. Introduction

MgO materials significantly impacted many industries due to its lower density, maximum strength-to-weight percentage, and high toughness [1]. Due to its poor physical properties, such as low tensile modulus, weak strength, absence of flexibility, maximum creep and wear, insufficient resistance to corrosion, and high susceptibility to fatigue, MgO was not used in industry [2, 3]. Researchers have put a lot of time and energy into developing alloys and composites of MgO with other elements including Cu, Ti, Al, TiO$_2$, ZnO, Al$_2$O$_3$, ZrO$_2$,

and TiC, to provide the flexibility and strength [4]. Magnesium oxide is one of the best biocompatible and biodegradable materials [5]. The medical industry uses stainless steel, Co-Cr and Ti. However, these materials produce poisonous by-products that are dangerous to the patient and necessitate expensive postoperative care once the patient has healed [6]. Including an appropriate reinforcement into the MgO matrix is one technique to get a material based on MgO with good mechanical characteristics for biomedical applications [7, 8]. The following improvement in the mechanical aspects of the MgO matrix depends on the reinforcement

uniformly distributed throughout the matrix [9]. Powder metallurgy, a mechanical alloying, permits consistent reinforcement distribution inside a matrix with either no interaction between the reinforcement and matrix or with only minimal interaction [10, 11].

Spark plasma sintering (SPS) is a new method used to consolidate powders [12]. This sintering method saves time over more conventional approaches since the powder is heated and compacted simultaneously to achieve high density with grain growth due to the rapid heating [13]. SPS can produce better mechanical properties than conventional sintering processes by reducing the sintering temperature and reducing the sintering time. Scientists have widely used SPS in producing various metals, ceramics, alloys, and composites [14]. Despite of its potential benefits, research on SPS for MgO-based composites is low [15, 16]. An in-situ composite comprising MgO and ZnO created by the author [17] used to enhance corrosion resistance in Hank's solution [18, 19].

Titanium carbide (TiC) is an extremely hard, strong, and thermally stable ceramic reinforcement [20, 21]. It has a melting point of 2790°C, a Rockwell hardness of 86 HRA, a Vickers hardness of 960 HV, a tensile modulus of 530 GPa [22]. Recently, TiC was mixed into an MgO matrix to improve its mechanical behaviors, creating it more appropriate for orthopedic uses [23]. An MgO-TiC composite with enhanced hardness and wear resistance has been developed by fusing powder metallurgy with the traditional sintering process [24, 25]. A MgO-TiC nanocomposite was fabricated by fragmented melt deposition, followed by heat treating, with the goal of improving mechanical characteristics such as yield strength, compressed elastic modulus, fracture stress, and base texture [26, 27]. However, no research has been identified so far that describes the production of MgO-3TiC composites using SPS, so the researchers chosen to develop this process.

Microhardness and density of MgO-3TiC composite studied in response to sintering factors, including temperature, pressure, and time. This MgO-3TiC composite's final mechanical and physical properties result from the interplay of multiple sintering parameters. As a result, the relative importance of each aspect in determining the composite qualities can be determined by using the Taguchi method.

2. Materials and Processing

The MgO used in this study has a particle size of $45\,\mu$m and purity of >99.8%. Titanium carbide (TiC) powder with a 99% purity and size of particles is $10\,\mu$m, was used to create the reinforcement. Through powder metallurgy synthesis, a pure MgO matrix creates and reinforced with TiC at a weight percentage of 3%. Powdered MgO and TiC blend in the appropriate proportions using a lower-energy milling machine, which ensured that the reinforcement dispersed throughout the matrix. The powder was mixed in Argon gas-filledstainless-steel vials by rotating them at 200 rpm for an hour. We used SPS to compact the milled powders (nine runs) at three distinct levels of sintering pressure, sintering temperature, and sintering time, following the L₉ OA shown in Table 1. Following consolidation, the sample was quickly

TABLE 1: Design of Taguchi **L₉** orthogonal arrays.

Specimen	Sintering temperature (°C)	Sintering pressure (MPa)	Sintering time (min)
1	500	35	15
2	500	45	20
3	500	55	25
4	550	35	20
5	550	45	25
6	550	55	15
7	600	35	25
8	600	45	15
9	600	55	20

removed from the die owing to a thin layer of graphite between the powder mixture and the die wall. In addition, the powder and die wall had less friction with this thin film. An internal thermocouple was positioned 2 mm from the center of the die's inner wall to measure the sintering temperature during consolidation. After being sintered, the samples were ground and polished to remove any remaining graphite [28]. All the grinding with SiC paper ranges in grit from 180, 320, 400, 600, and 800. The next step was polishing using alumina slurry. The specimens in an ethanol solution and washed with digital ultrasonicator for 15 min to remove the alumina particles that adhered to the composites throughout this polishing process.

3. Experimental Procedures

3.1. Design of Experiments. To overcome the constraints of traditional optimization techniques, the design of experiments (DOE) method is now frequently used [29]. The Taguchi method found a fractional factorial design to optimize process parameters, such as experimental time and cost, and the complete factorial design by the strategic selection [30, 31]. The Taguchi method uses the S/N ratio and an orthogonal array (OA) to determine the optimal settings for the controllable variables. According to the objective, the optimal size of the S/N ratio might range from large to nominal to small.

In this study, a statistical analysis assuming that greater values are better since we found that increased microhardness and experimental density are all desirable. The optimum S/N ratio calculates using the following equation, where a higher value is preferred.

$$\frac{S}{N} = -10 \log \frac{1}{n} \left(\sum_{i=1}^{n} \frac{1}{y_i^2} \right). \tag{1}$$

Orthogonal arrays are only possible when the total number of parameters exceeds the sum of the parameters [32, 33]. This investigation considers three parameters, each of which has three stages in the tests: 500, 550, and 600°C for sintering temperature; 35, 45, and 55 MPa for sintering pressure; and 15, 20, and 25 min for sintering time. For this purpose, we decided on a L₉ orthogonal array (Table 1). Experiments were performed with three different sintering parameters: sintering temperature, pressure, and time.

3.2. Characterization. Cu-Kα radiation with the wavelength $\lambda = 1.54056$ Å, and a scan speed of $2°$/min is used to conduct XRD analysis on as-received powders, processed MgO-3TiC powder, and sintered specimens. With the help of Archimedes' principle, the densities of SPS MgO-3TiC composite specimens were examined. The samples were first measured in the air using a digital meter of ±0.00001 g and then reweighed in distilled water. Here, we give the mean density readings from five independent measurements. To theoretically determine the completed composites' density, we applied the rule-of-mixture approach. Researchers looked into the surface shape and distribution of the TiC reinforcing in MgO-3TiC composites. The microstructure of SPS specimens was analyzed using FE-SEM and an SEM.

The hardness was measured using a Vickers diamond pyramid indenter at an angle of $136°$ and a universal hardness tester. After being loaded at 200 gf, the sample was given a 10-second dwell time. According to the ISO 6507/ASTM E384 specifications, the average of five separate HV readings were analyzed. Metallographically polished samples were subjected to an HR test using a universal hardness tester. In this study, 10 sec dwell period was used gives the average HR from five separate tests.

4. Results and Discussion

4.1. X-ray Diffraction Analysis. Using XRD characterization, the impact of TiC on the crystalline structure of the pure MgO matrix was analyzed. To form MgO-TiC composites, the wettability between the MgO and TiC matrix reinforcement must be high [34]. Due to the interaction between the TiC reinforcement and the MgO's crystalline structure, the MgO's base texture was altered. Figure 1 shows the normalized XRD patterns of MgO powder, TiC powder, a milled MgO-3TiC [35] composite, and a spark-plasma-sintered composite. The distinct peaks of the MgO and TiC powders are highly noticeable. However, only the MgO peak is visible in the MgO-3TiC composite. Because of the low concentration of TiC (3 wt %), the corresponding peaks are present but weaker in intensity. The results for the SPS specimen at high temperatures corroborate the presence of TiC in the manufactured composite. TiC specimens sintered at $550°$C and $600°$C show the first peak. The additional peaks may be discernible at lower intensities. SPS specimens' XRD spectra show no unexpected peaks, indicating no distinctive phases generated during the sintering. This finding further substantiates the viability of the SPS technique for manufacturing MgO-3TiC composites.

4.2. SEM Characterization. SEM micrographs of the MgO (Figure 2(a)), TiC (Figure 2(b)), Both powders were received in an uneven shape and an extensive size range. Figure 2(a), reveals a particle size distribution in the MgO matrix. In contrast, Figure 2(b) is an electron image of the TiC reinforcement, shows more uniform particle size. No agglomerated big particles were visible when standard sintering was combined with cold compaction.

Micrographs taken with an FE-SEM revealed reinforcement dispersed throughout the matrix of spark-plasma-sintered samples. The specimens had no apparent porosity when using an FE-SEM following SPS. This finding demonstrates the efficacy of the spark plasma sintering technique in creating dense models. TiC dispersed in the MgO matrix, and FE-SEM micrographs revealed the enhanced interfacial integrity. Increased interfacial integrity among the reinforcement and matrix allowed all sintered samples to be free from debonding and voids. Micrographs also revealed that the MgO-3TiC composites showed no micropores or shrinkage. All of the MgO-3TiC specimens indicate as FE-SEM micrographs in Figure 3. Firm adhesion evidence by the support of maintaining a fixed location within the matrix. In comparison to pure MgO matrices, MgO-3TiC composites will exhibit sufficient resistance to indentation due to the strong adherence of reinforcements.

The Scherrer equation was used to find out the size of the crystallites in the MgO powders, the TiC reinforcements, and the sintered specimens of the resulting composites. The MgO powder and the TiC reinforcement crystallite sizes are of ~36 nm and ~40 nm. The sintered MgO-3wt%TiC composite samples showed a range of crystallite sizes from ~30 nm to ~42 nm, depending on the varied sintering settings used. Spark plasma sintering results in small to no grain development, as evidenced by the small size distribution range of the crystallites.

4.3. Impact of Input Factors on Microhardness. The purpose of this study is to determine which variables and their interactions have the greatest impact on the microhardness of MgO-3TiC composites. Table 1 displays the microhardness measurements made and the L$_9$ orthogonal array from the Taguchi design. At least five replicates of each experiment perform to ensure statistical significance. There were nine trials to analyze the S/N ratio and to learn how uncontrollable factors affected the sintering process. Results were confirmed using the signal-to-noise ratio. Main effect plots for the mean microhardness display in Figure 4(a) and the results of S/N ratio is indicated in Figure 5.

These graphs show the typical results of each experiment and can be used to efficiently look into how different variables affect the mechanical qualities. According to Table 2, the maximum microhardness attains at a sintering temperature of $550°$C. Due to localized matrix deformation during indentation, the MgO matrix's hardness was increased upon the addition of the tougher TiC reinforcement. Microhardness increased from 500 to $550°$C, with the rise at $550°$C attributable to a greater degree of densification as depicted in Figure 3. Raising the SPS temperature speeds up the process of elimination, to increase the density and hardness [36, 37].

However, the composite's microhardness appeared to decrease at $600°$C. Increased grain size during processing at high temperatures clarifies the results [38]. A higher sintering pressure of 55 MPa or more causes plastic deformation, which causes the grains to shrink and the microhardness to rise. With the influence of sintering
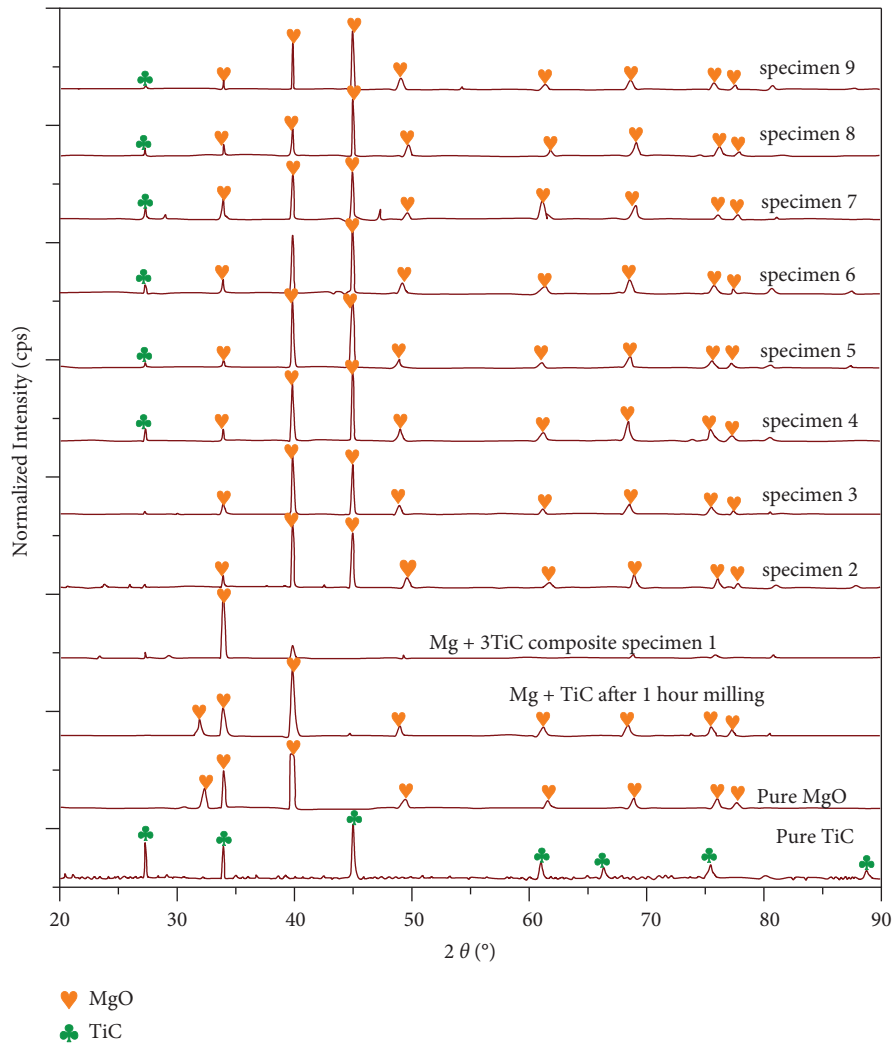
Figure 1: X-ray diffraction.
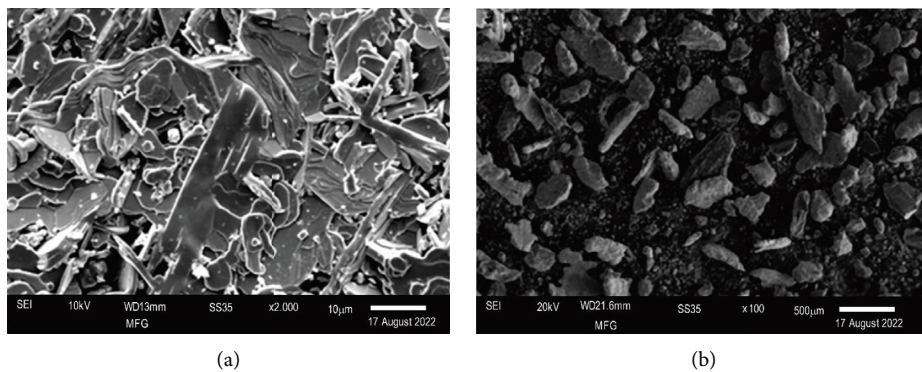
Figure 2: SEM images of (a) MgO and (b) TiC.

temperature, sintering periods of 25 minutes resulted in grain formation and led to lower HV.

An ANOVA was used to determine the process factor impacted the microhardness. ANOVA is used to find out the significant difference between three or more mean values. Results from this method, computed with Minitab 16 at a 95% confidence range (significant level $\alpha = 0.05$), are shown in Tables 3 and 4. The microhardness ANOVA results summarize in Table 3, and the sound-to-noise ratio ANOVA outcomes confirms in Table 4.

The microhardness of the MgO-3TiC composite was importantly impacted by all of the sintering factors listed in
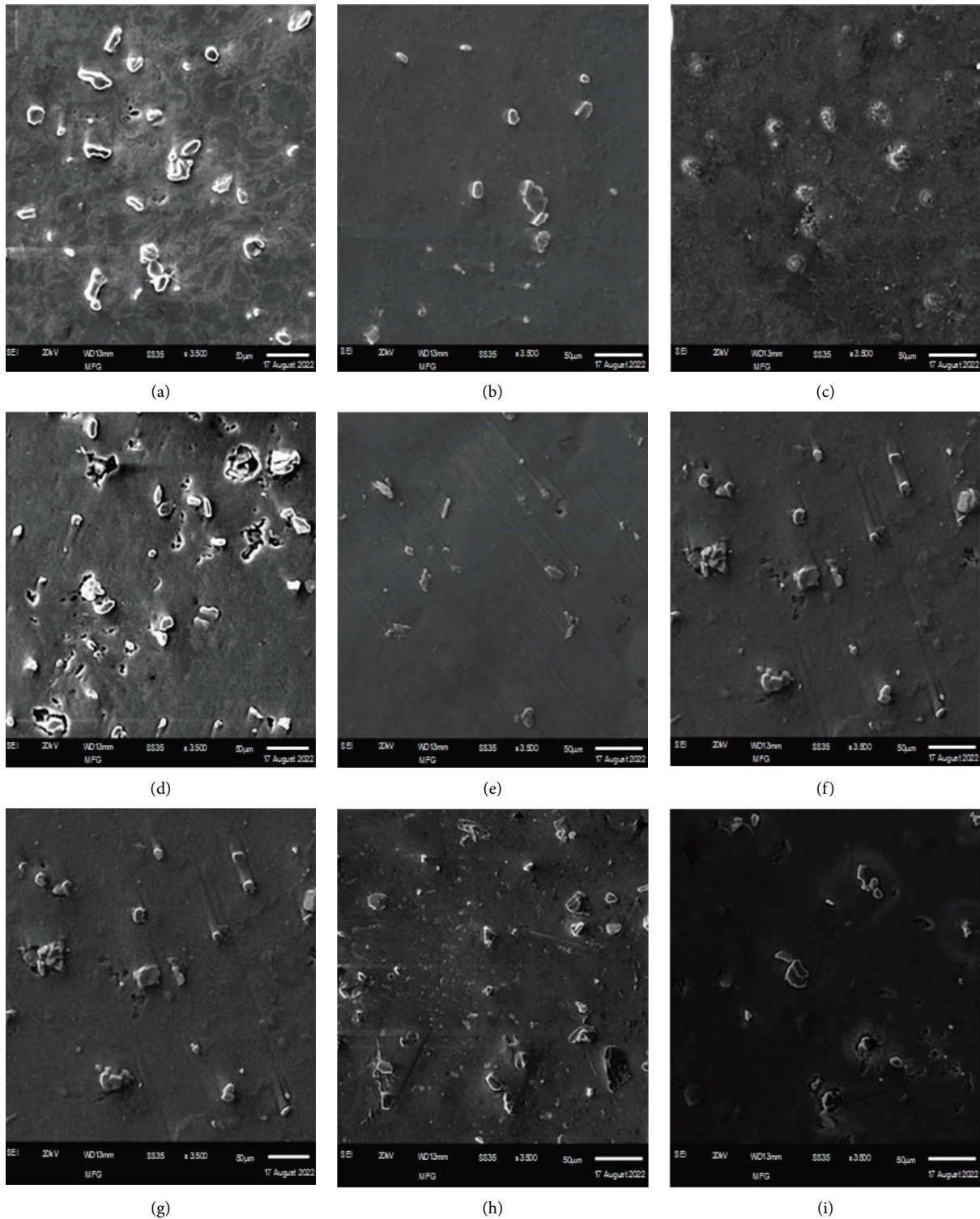
FIGURE 3: SEM micrographs of SPS specimen (a) specimen 1, (b) specimen 2, (c) specimen 3, (d) specimen 4, (e) specimen 5, (f) specimen 6, (g) specimen 7, (h) specimen 8, and (i) specimen 9.

Table 3, as evidenced by p values <0.05. The most significant sintering factor is temperature ($p = 0.001$), followed by sintering time ($p = 0.005$) and sintering pressure ($p = 0.07$). From this, we can conclude that all the sintering parameters significantly impacted the measured microhardness.

The importance of specific variables was confirmed by the analysis of p value. It is used to find the different variables interact with one another. A smaller p value represents a more substantial effect of the factor on the process. The sum of squares and the F value together can help you identify
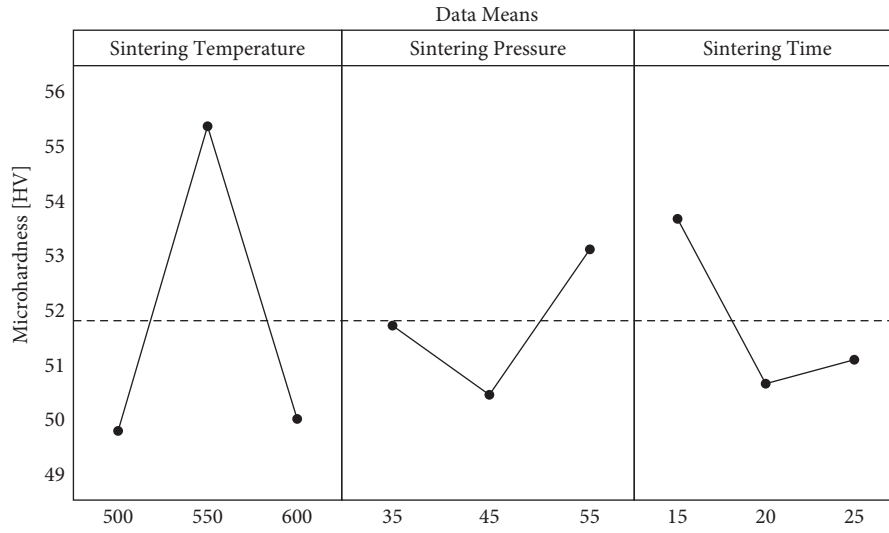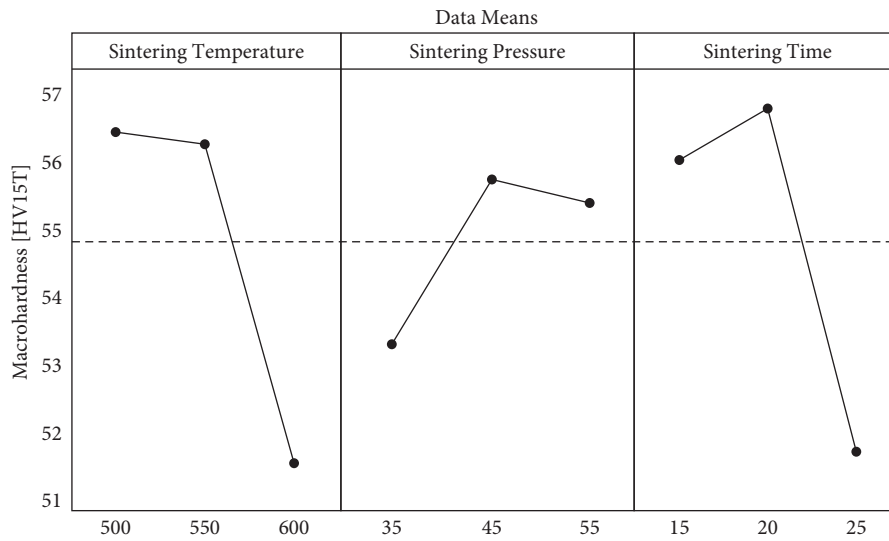
FIGURE 4: Impact of processing factors on (a) microhardness, (b) macrohardness, and (c) experimental density.

Main Effects Plot for S/N ratios
Data Means
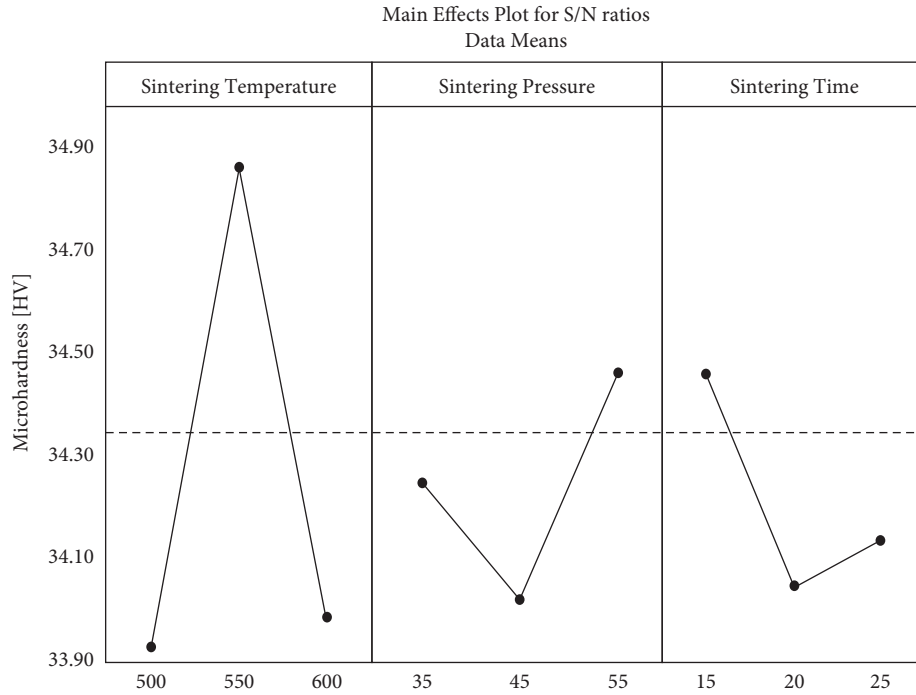
FIGURE 5: Effect of processing parameters on S/N ratio of microhardness.

TABLE 2: Results of experiments sorted by sintering factors for mean microhardness HV and signal-to-noise.

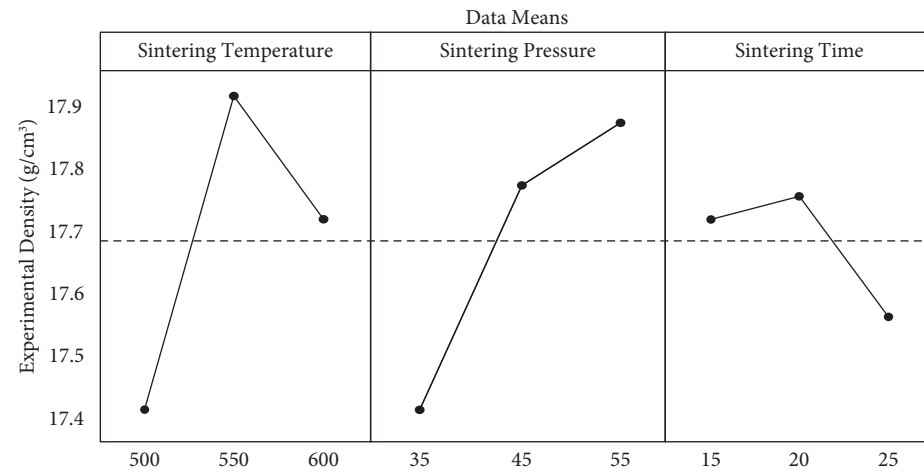|	Sintering factors			Responses	
Experimental run	Sintering temperature	Sintering pressure	Sintering time	Mean MH	Mean signal to noise ratio
	(°C)	(MPa)	(min)	(HV)	(dB)
1	500	35	15	51.41	34.2140
2	500	45	20	47.01	33.4421
3	500	55	25	50.41	34.0487
4	550	35	20	54.21	34.6801
5	550	45	25	53.21	34.5183
6	550	55	15	58.61	35.3581
7	600	35	25	49.01	33.8040
8	600	45	15	50.61	34.0831
9	600	55	20	50.01	33.9795

TABLE 3: ANOVA analysis for the mean of microhardness.

ANOVA response table for microhardness						
Source	DF	Seq SS	Adj SS	Adj MS	F values	P values
Sintering temperature (°C)	2	62.828	62.828	31.414	785.34	0.002
Sintering pressure (MPa)	2	11.228	11.228	5.614	140.34	0.008
Sintering time (min)	2	17.148	17.148	8.574	214.34	0.006
Error	2	0.081	0.081	0.041		
Total	8	91.281				

Ranking response table for microhardness			
Level	Sintering temperature (°C)	Sintering pressure (MPa)	Sintering time (min)
1	49.61	51.54	53.54
2	55.34	50.28	50.41
3	49.88	53.01	50.88
Delta	5.74	2.74	3.14
Rank	1	3	2

TABLE 4: ANOVA analysis for the S/N ratio of microhardness.

ANOVA response table for the S/N ratio						
Source	DF	Seq SS	Adj SS	Adj MS	*F* values	*P* values
Sintering temperature (°C)	2	1.70683	1.70683	0.853411	236.61	0.005
Sintering pressure (MPa)	2	0.30054	0.30054	0.150267	41.667	0.024
Sintering time (min)	2	0.46283	0.46283	0.231413	64.17	0.016
Error	2	0.00722	0.00722	0.003608		
Total	8	2.47740				
Ranking response table for the S/N ratio						
Level		Sintering temperature (°C)		Sintering pressure (MPa)		Sintering time (min)
1		33.91		34.24		34.56
2		34.86		34.02		34.04
3		33.97		34.47		34.13
Delta		0.96		0.46		0.53
Rank		1		3		2

the most critical factor. In addition, ANOVA ranks the sintering parameters according to how well they provide the desired average microhardness and average S/N ratio. Separate values determine a final test statistic denoted by the term "degree of freedom (DoF)." When one or more independent variables add to a regression model, the error sum of squares (Seq SS) decreases. The *p* value determines by calculating the Adj SS, a measure of the dispersion of the model or terms. Minitab uses the Adj MS, which measures the degree of variance in a specified period or model to compute *p* values.

4.4. Influence of Input Parameters on Macrohardness.
Table 5 displays the L$_9$ orthogonal array for the Rockwell test's for macrohardness HR15T measurement. Table 6 confirms the results for the mean and ranking of variables for macrohardness, and Table 7 supports the main effect plots for macrohardness signal-to-noise ratio and ranking. The main effect plots for the average macrohardness are depicted in Figure 4(b), while the main effect plots for the S/N ratio to confirm the results, are shown in Figure 6. The macrohardness shows minor fluctuations between 500 and 600°C, and its value drops dramatically with subsequent increases in sintering temperature. Higher grain growth at elevated temperatures explains this effect.

The Hall–Petch relationship uses materials in which macrohardness decreases with increasing grain size. Higher temperatures promote dislocation migration and destruction, resulting in a lower dislocation density in the material. Increases in both the sintering pressure and the plastic deformation resulting leads to increased quantity and density of dislocations the greater the number of dislocations, the smaller the resulting grains, and the greater the macrohardness. However, the opposite impact shows the combining pressures more significant than 45 MPa with extended sintering times, leads to increased grain size. After 20 minutes of sintering, the macrohardness reached a maximum of 60.248 HV. Considerable grain growth may have contributed to this result due to the lengthy exposure to the hot conditions [39].

4.5. Influence of Input Parameters on Density.
Table 8 displays the S/N ratio and the L$_9$ orthogonal array derived from the Taguchi method to measure the ED with Archimedes' principle. In addition, Table 8 displays the theoretical density (TD) and standard deviation of the density for the composite.

Figure 4(c) depicts the main effect graphs for the mean density, while Figure 7 indicates S/N ratio. Figure 4(c) shows that as sintering temperatures increased but the density decreased. Solid particles melt and diffuse more quickly at 550°C the MgO-3TiC composite displays this typical behavior. The density reduced as the sintering temperature raise from 500 to 600°C, inflating the prepared composite. There is a correlation between the increased density (4.52 g/cm^3) of the TiC strengthening and the enhanced composite density [40]. The increased density demonstrates the feasibility of using the SPS consolidation

TABLE 5: Results of experiments sorted by sintering variables for mean macrohardness and signal-to-noise.

Experimental run	Sintering factors			Responses	
	Sintering temperature (°C)	Sintering pressure (MPa)	Sintering time (min)	Mean macrohardness (HR)	Mean S/N ratio (dB)
1	500	35	15	62.191	35.8747
2	500	45	20	50.632	34.0883
3	500	55	25	56.853	35.0957
4	550	35	20	59.623	35.5074
5	550	45	25	60.191	35.5898
6	550	55	15	49.373	33.8691
7	600	35	25	37.881	31.5673
8	600	45	15	56.526	35.0445
9	600	55	20	60.254	35.5996

TABLE 6: ANOVA analysis for the mean of macrohardness.

ANOVA response table for macrohardness						
Source	DF	Seq SS	Adj SS	Adj MS	F values	P values
Sintering temperature (°C)	2	48.51	48.51	24.31	0.14	0.885
Sintering pressure (MPa)	2	11.71	11.71	5.91	0.04	0.970
Sintering time (min)	2	46.91	46.91	23.41	0.14	0.889
Error	2	369.91	369.91	185.01		
Total	8	477.11				

Ranking response table for macrohardness			
Level	Sintering temperature (°C)	Sintering pressure (MPa)	Sintering time (min)
1	56.56	53.23	56.03
2	56.40	55.79	56.84
3	51.56	55.50	51.65
Delta	5.02	2.56	5.20
Rank	2	3	1

TABLE 7: ANOVA analysis for the mean S/N ratio of macrohardness.

ANOVA response table for the S/N ratio						
Source	DF	Seq SS	Adj SS	Adj MS	F values	P values
Sintering temperature (°C)	2	1.7455	1.7455	0.8728	0.17	0.861
Sintering pressure (MPa)	2	0.6424	0.6424	0.3212	0.07	0.944
Sintering time (min)	2	1.6943	1.6943	0.8472	0.17	0.864
Error	2	10.7066	10.7066	5.3533		
Total	8	14.7884				

Ranking response table for the S/N ratio			
Level	Sintering temperature (°C)	Sintering pressure (MPa)	Sintering time (min)
1	35.03	34.33	34.94
2	35.00	34.92	35.07
3	34.01	34.86	34.09
Delta	0.96	0.60	0.99
Rank	2	3	1

strategy used in this study to produce dense components. At 550°C, the density has a slight standard deviation, suggesting that the TiC reinforcement is dispersed evenly throughout the MgO matrix. When applying the innovative SPS consolidation method with the precise parameter values listed in Table 8, porosity of 0.23% or below is easily achievable. The experimental density of the composites rises with sintering pressure, as shown in Figure 4(c). The solid composite powder's volume decreased, which led to this result.
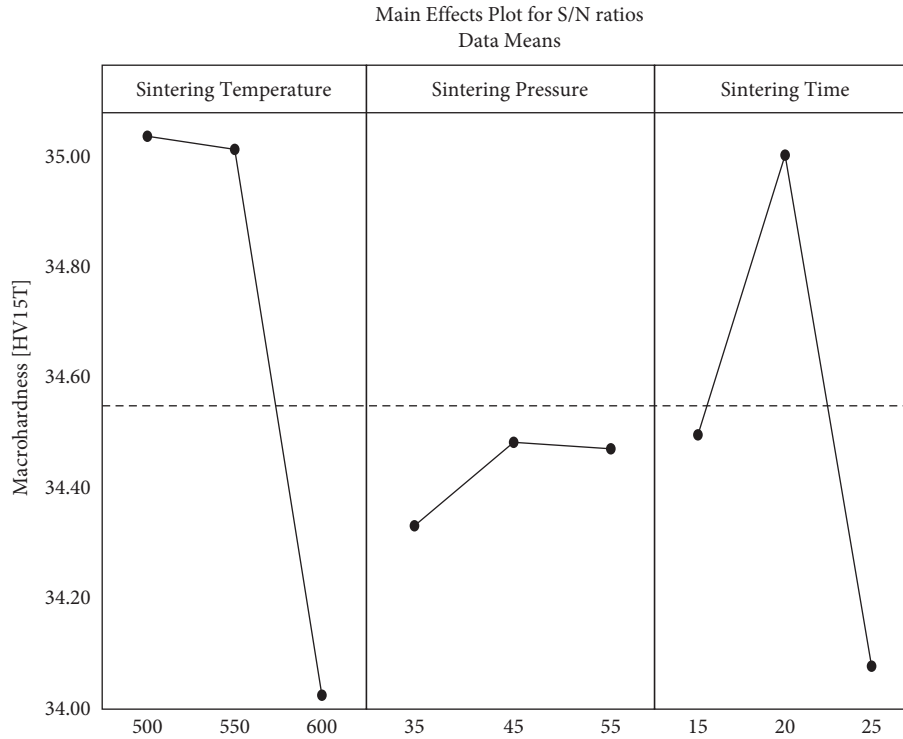
Main Effects Plot for S/N ratios
Data Means

FIGURE 6: Effect of processing parameters on S/N ratio of macrohardness.

In addition, the intergranular pore's fill and density increased by increasing the pressure applied during the sintering process. Like the effect of temperature, sintering duration has a modest but noticeable impact on the experimental density of MgO-3TiC. Since there was not enough time for the molecules to diffuse, the initial density was lower and the porosity was higher due to the spaces between the particles [41]. However, with 20 minutes of sintering time, the dispersion was sufficient to close any remaining pores and increase the test densities with slight variations in volume. The composite material exposes to high temperatures for even longer when the sintering time extends to 25 minutes. Because of this, the composite grew in size and lost density. Tables 9 and 10 display the results of the ANOVA test for the signal-to-noise ratio, and mean results for the experimental density, respectively. It was concluded that none of the process parameters or the signal-to-noise ratio played a significant role in the observed scatter in the MgO-3TiC microcomposite densities experiments because their p values are more important than the 95% confidence interval. Many variables affected the experimental density, but sintering pressure and sintering time had the most significant impacts [42]. The sintering temperature ($p = 0.229$) had the slightest influence on all the insignificant variables affecting the composite experimental density.

TABLE 8: Results from experiments sorted by sintering parameters, with emphasis on mean density and signal-to-noise ratio.

| Experimental run	Sintering factor's				Responses (experimental density, *S/N* ratio)			
	Sintering temperature (°C)	Sintering pressure (MPa)	Sintering time (minutes)	TD (g/cm^3)	Mean ED (g/cm^3)	SD	Porosity (%)	Mean signal to noise ratio (dB)
1	500	35	15	1.81	1.721	0.035767	4.57	4.73617
2	500	45	20	1.81	1.741	0.002110	3.57	4.82660
3	500	55	25	1.81	1.761	0.025828	2.165	4.95175
4	550	35	20	1.81	1.781	0.003175	1.07	5.04905
5	550	45	25	1.81	1.791	0.000412	0.45	5.10270
6	550	55	15	1.81	1.801	0.001626	0.26	5.11976
7	600	35	25	1.81	1.721	0.014249	4.75	4.71977
8	600	45	15	1.81	1.791	0.000657	4.57	5.07017
9	600	55	20	1.81	1.801	0.001820	3.57	5.11514

Main Effects Plot for S/N ratios
Data Means
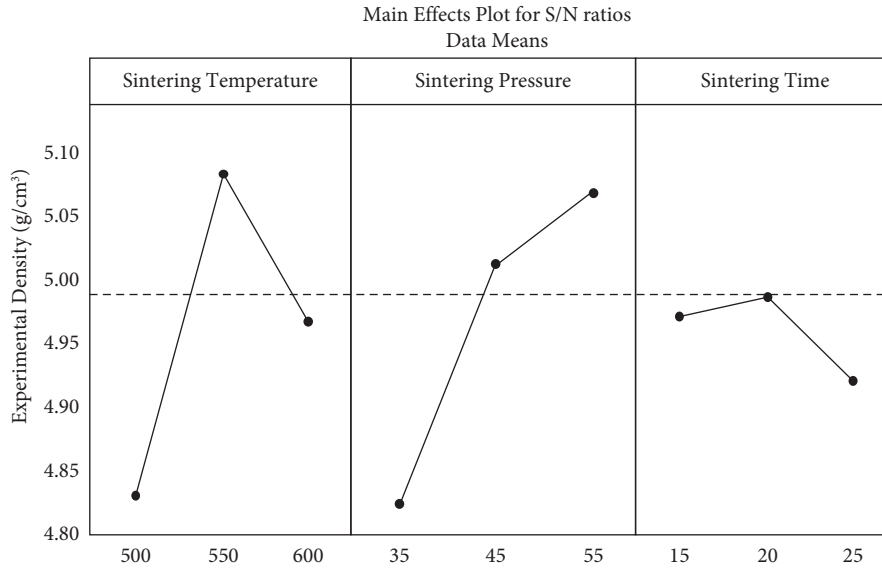
Figure 7: Effect of processing parameters on S/N ratio of experimental density.

Table 9: ANOVA analysis for the mean of experimental density.

ANOVA response table for experimental density						
Source	DF	Seq SS	Adj SS	Adj MS	F values	P values
Sintering temperature (°C)	2	0.0039603	0.0039603	0.0019802	3.37	0.230
Sintering pressure (MPa)	2	0.0033939	0.0033939	0.0016970	2.89	0.259
Sintering time (min)	2	0.0003386	0.0003386	0.0001693	0.30	0.778
Error	2	0.0011793	0.0011793	0.0005897		
Total	8	0.0088719				
Ranking response table for experimental density						
Level		Sintering temperature (°C)		Sintering pressure (MPa)		Sintering time (min)
1		1.741		1.746		1.775
2		1.791		1.779		1.779
3		1.771		1.792		1.764
Delta		0.052		0.047		0.016
Rank		1		2		3

Table 10: ANOVA analysis for the mean S/N ratio of experimental density.

ANOVA response table for the S/N ratio						
Source	DF	Seq SS	Adj SS	Adj MS	F values	P values
Sintering temperature (°C)	2	0.09555	0.09555	0.04778	3.31	0.233
Sintering pressure (MPa)	2	0.08270	0.08270	0.04135	2.87	0.260
Sintering time (min)	2	0.00825	0.00825	0.00413	0.29	0.779
Error	2	0.02895	0.02895	0.01448		
Total	8	0.21542				
Ranking response table for the S/N ratio						
Level		Sintering temperature (°C)		Sintering pressure (MPa)		Sintering time (min)
1		4.839		4.836		4.976
2		5.091		5.001		4.998
3		4.969		5.063		4.926
Delta		0.253		0.228		0.073
Rank		1		2		3

5. Conclusion

Spark plasma sintering (SPS) is used to create an MgO metal matrix composite. Sintering temperature, sintering pressure, and sintering Time were studied using Taguchi analysis to certain impact on the MgO composites' physical and mechanical characteristics. It is possible to infer the following from this study:

(1) Through spark plasma sintering, a metal matrix composite based on magnesium oxide and strengthened with 3% TiC.

(2) Micrographs taken with an FE-SEM indicated no apparent porosity, and TiC was distributed relatively uniformly throughout the MgO matrix, as determined by the microstructural study. When comparing the TiC-reinforced material to a pure MgO matrix, the results showed an increase in hardness due to the reinforcement.

(3) All of the sintering process had a considerable impact on microhardness. Microhardness primarily affected by sintering temperature, with sintering time and pressure.

(4) The macrohardness of the manufactured composite was little affected by any of the sintering conditions.

Data Availability

All authors confirmed that all necessary data are available in this manuscript.

Conflicts of Interest

The authors declare that they have no conflicts of interest.

References

[1] C. Goswami, I. K. Bhat, A. Patnaik, T. Singh, and G. Fekete, "Fabrication of ceramic hip implant composites: influence of silicon nitride on physical, mechanical and wear properties," *Silicon*, vol. 12, no. 5, pp. 1237–1245, 2020.

[2] M. A. Alam, H. H. Ya, M. Yusuf et al., "Modeling, optimization and performance evaluation of tic/graphite reinforced al 7075 hybrid composites using response surface methodology," *Materials*, vol. 14, pp. 4703–4716, 2021.

[3] M. Kazemi, H. Saghafian, and M. Hooshyar, "Evaluating the impacts of laser process parameters on microstructure and microhardness of H13-TiC composite using the mathematical modelling," *SN Applied Sciences*, vol. 2, no. 12, p. 1942, 2020.

[4] A. H. Nassajpour-Esfahani, A. Bahrami, A. Alhaji, and R. Emadi, "Optimization of slip casting parameters for spark plasma sintering of transparent MgAl2O4/Si3N4 nanocomposite," *Ceramics International*, vol. 45, no. 16, pp. 20714–20723, 2019.

[5] A. Esmaeilzaei, S. A. Sajjadi, S. Mollazadeh Beidokhti, and H. Beygi, "Rapid consolidation of Al2O3-TiO2-Co nanocermets via spark plasma sintering of Co-coated ceramic particles," *Journal of Alloys and Compounds*, vol. 771, pp. 79–88, 2019.

[6] J. Hojo, "Ceramics powder processing: design of particle structure toward development of sintered texture and functions," *Journal of the Japan Society of Powder and Powder Metallurgy*, vol. 63, no. 9, pp. 801–810, 2016.

[7] S. Jaiswal, A. Dubey, S. Haldar, P. Roy, and D. Lahiri, "Differential in vitro degradation and protein adhesion behaviour of spark plasma sintering fabricated magnesium-based temporary orthopaedic implant in serum and simulated body fluid," *Biomedical Materials*, vol. 15, no. 1, Article ID 15006, 2019.

[8] C. S. Lee, H. C. Lee, G.-H. Kim, J. H. Han, W. J. Kim, and H. S. Kim, "Design of Mg-6wt%Al alloy with high toughness and corrosion resistance prepared by mechanical alloying and spark plasma sintering," *Materials Characterization*, vol. 158, Article ID 109995, 2019.

[9] Š. Csáki, F. Lukáč, J. Veverka, and T. Chraska, "Preparation of Ti3SiC2 MAX phase from Ti, TiC, and SiC by SPS," *Ceramics International*, vol. 48, no. 19, pp. 28391–28395, 2022.

[10] R. Liu, W. Wang, H. Chen, Z. Lu, W. Zhao, and T. Zhang, "Densification of pure magnesium by spark plasma sintering-discussion of sintering mechanism," *Advanced Powder Technology*, vol. 30, no. 11, pp. 2649–2658, 2019.

[11] R. Pournajaf, S. A. Hassanzadeh-Tabrizi, R. Ebrahimi-Kahrizsangi, A. Alhaji, and A. A. Nourbakhsh, "Polycrystalline infrared-transparent MgO fabricated by spark plasma sintering," *Ceramics International*, vol. 45, no. 15, pp. 18943–18950, 2019.

[12] O. A. Lukianova, A. N. Khmara, S. N. Perevislov, D. A. Kolesnikov, and V. Krasilnikov, "Electrical resistivity of silicon nitride produced by various methods," *Ceramics International*, vol. 45, no. 7, pp. 9497–9501, 2019.

[13] S. D. Oguntuyi, N. Malatji, M. B. Shongwe, O. T. Johnson, C. Khoathane, and L. Tshabalala, "The influence of Si3N4 on the microstructure, mechanical properties and the wear performance of TiB2–SiC synthesized via spark plasma sintering," *International Journal of Lightweight Materials and Manufacture*, vol. 5, no. 3, pp. 326–338, 2022.

[14] Z. Ma, H. Cheng, J. Fan, Z. Wang, and Z. Liu, "Effect of Mo and TiC addition on the microstructure and mechanical properties of spark plasma sintered Si3N4 composites," *Ceramics International*, vol. 48, no. 15, pp. 22362–22369, 2022.

[15] R. Halder and S. Bandyopadhyay, "Spark plasma sintering of nano magnesia: processing parameters influencing optical properties," *Materials Chemistry and Physics*, vol. 228, pp. 51–59, 2019.

[16] C. Goswami, I. K. Bhat, S. Bathula, T. Singh, and A. Patnaik, "Physico-mechanical and surface wear assessment of magnesium oxide filled ceramic composites for hip implant application," *Silicon*, vol. 11, no. 1, pp. 39–49, 2019.

[17] Y. Xiong, H. Li, J. Huang, Z. Ye, and J. Yang, "Fabrication of TiC coated short carbon fiber reinforced Ti3SiC2 composites: process, microstructure and mechanical properties," *Journal of the European Ceramic Society*, vol. 42, no. 9, pp. 3770–3779, 2022.

[18] M. Shahedi Asl, Z. Ahmadi, F. Sadegh Moghanlou, M. Vajdi, and M. Shokouhimehr, "Nanocharacterization of spark plasma sintered TiB2–SiC–graphene composites," *Materials Characterization*, vol. 189, Article ID 111986, 2022.

[19] F. S. Hamid, O. A. E. El-Kady, A. R. S. Essa, A. E. G. El-Nikhaily, A. Elsayed, and W. Abd-Elaziem, "Synthesis and characterization of titanium carbide and/or alumina nanoparticle reinforced copper matrix composites by spark plasma sintering," *Journal of Materials Engineering and Performance*, vol. 31, no. 7, pp. 5583–5592, 2022.

[20] O. S. Kryzhanovska, "Y203-MgO highly-sinterable nano-powders for transparent composite ceramics," *Metallic Functional Materials*, vol. 26, no. 4, pp. 829–837, 2019.

[21] Y. Pristinskiy, N. Washington Solis Pinargote, and A. Smirnov, "The effect of MgO addition on the microstructure and mechanical properties of alumina ceramic obtained by spark plasma sintering," *Materials Today Proceedings*, vol. 19, pp. 1990–1993, 2019.

[22] T. M. Vidyuk, D. V. Dudina, M. A. Korchagin et al., "Spark plasma sintering treatment of cold sprayed materials for synthesis and structural modification: a case study using TiC-Cu composites," *Materials Letters X*, vol. 14, Article ID 100140, 2022.

[23] P. Satishkumar, C. Saravana Murthi, R. Chebolu et al., "Optimizing the mechanical and microstructure characteristics of stir casting and hot-pressed AA 7075/ZnO/ZrO2 composites," *Advances in Materials Science and Engineering*, vol. 2022, Article ID 6559014, 18 pages, 2022.

[24] S. M. Mirbagheri, H. Shahrajabian, and M. Rafiei, "Effects of graphene nanoplatelets on the microstructure, mechanical properties, and corrosion behavior of spark plasma sintered Al + 20 vol.% (TiC + TiB2) hybrid composites," *Journal of Materials Engineering and Performance*, vol. 31, no. 5, pp. 3535–3549, 2022.

[25] D. Garbiec, A. M. Laptev, V. Leshchynsky et al., "Spark plasma sintering of WC-Ti powder mixtures and properties of obtained composites," *Journal of the European Ceramic Society*, vol. 42, no. 5, pp. 2039–2047, 2022.

[26] S. Ramesh, K. Y. Sara Lee, and C. Y. Tan, "A review on the hydrothermal ageing behaviour of Y-TZP ceramics," *Ceramics International*, vol. 44, no. 17, pp. 20620–20634, 2018.

[27] O. A. Lukianova, V. V Krasil'Nikov, R. E. Bogachev, A. A. Parkhomenko, and A. I. Kartamyshev, "Effect of Various Additives and Method of Sintering on the Silicon Nitride Phase Transformation," in *Proceedings of the 2018 IEEE 8th International Conference Nanomaterials: Application & Properties (NAP)*, Zatoka, Ukraine, September 2018.

[28] A. A. Parkhomenko, O. A. Lukianova, A. N. Khmara, and V. V Krasil'Nikov, "Effect of the various oxide additives on the microhardness of silicon nitride ceramics," in *Proceedings of the 2017 IEEE 7th International Conference on Nanomaterials Applications and Properties NAP 2017*, Odessa, UKraine, September 2017.

[29] K. S. Ali, R. Karunanithi, M. Prashanth, S. Sivasankaran, B. Subramanian, and H. S. Jailani, "Structure and mechanical properties of in-situ synthesized α-Ti/TiO2/TiC hybrid composites through mechanical milling and spark plasma sintering," *Ceramics International*, vol. 48, no. 8, pp. 11215–11227, 2022.

[30] V. Nečina and W. Pabst, "Electric current assisted sintering of ceramics - steps and pitfalls on the way to transparency," in *Polycrystalline Materials: Synthesis, Performance and Applications* Nova Science Publishers, Hauppauge, NY, USA, 2018.

[31] O. A. Lukianova and O. N. Ivanov, "The effect of Al2O3-MgO additives on the microstructure of spark plasma sintered silicon nitride," *Ceramics International*, vol. 44, no. 1, pp. 390–393, 2018.

[32] R. Zhang, B. Chen, F. Liu, M. Sun, H. Zhang, and C. Wu, "Microstructure and mechanical properties of composites obtained by spark plasma sintering of Ti3SiC2-15 vol.%Cu mixtures," *Materials*, vol. 15, pp. 2515–2517, 2022.

[33] H. M. A. Mahmoud, P. Satishkumar, Y. S. Rao et al., "Investigation of mechanical behavior and microstructure analysis of AA7075/SiC/B4C-based aluminium hybrid composites," *Advances in Materials Science and Engineering*, vol. 2022, Article ID 2411848, 10 pages, 2022.

[34] L. Liu, C. Cui, H. Geng et al., "Refining and reinforcing effects of TiC-Al2O3/Al ribbons inoculant on Al-Si-Mg-Ti alloy," *Materials Research Express*, vol. 9, no. 3, Article ID 036516, 2022.

[35] S. N. Grigoriev, Y. Pristinskiy, T. N. Soe et al., "Processing and characterization of spark plasma sintered SiC-TiB2-TiC powders," *Materials*, vol. 15, pp. 1946–1955, 2022.

[36] D. Sharma, V. K. Singla, and S. Singh, "Effect of multi-layer graphene on microstructure and mechanical properties of titanium-based composites," *Proceedings of the Institution of Mechanical Engineers - Part C: Journal of Mechanical Engineering Science*, vol. 236, no. 15, pp. 8542–8551, 2022.

[37] P. Satishkumar, N. Natarajan, R. Saminathan et al., "Investigation of mechanical and tribological properties of AA6061/MWCNT/B 4 C hybrid metal matrix composite," *Advances in Materials Science and Engineering*, vol. 2022, Article ID 1684169, 8 pages, 2022.

[38] K. L. Meena, S. Mozammil, and T. S. Srivatsan, "Development of Zirconia Toughend Nanocomposites Using the Technique of Spark Plasma Sintering: Role of Reinforcement," *Minerals, Metals And Materials Series*, Springer, Berlin, Germany, 2022.

[39] I. V. Kozerozhets, G. P. Panasyuk, L. A. Azarova et al., "Acquisition, properties, and application of nanosized magnesium oxide powders: an overview," *Theoretical Foundations of Chemical Engineering*, vol. 55, no. 6, pp. 1126–1132, 2021.

[40] A. A. Popov, M. S. Boldin, A. V. Nokhrin, and V. N. Chuvil'Deev, "The effect additives of magnesium, titanium and zirconium oxides additives on the densification kinetics and structure of alumina during spark plasma sintering," *IOP Conference Series: Materials Science and Engineering*, vol. 1014, Article ID 012045, 2021.

[41] Z. Feng, Y. Zhang, J. Tan et al., "Large strain hardening of magnesium containing in situ nanoparticles," *Nanotechnology Reviews*, vol. 10, no. 1, pp. 1018–1030, 2021.

[42] P. Satishkumar and N. Natarajan, "Investigation of mechanical properties and abrasive assisted electrochemical machining parameters on Al6061-10%TiB2-3% Gr hybrid ceramic composite," *Journal of Ceramic Processing Research*, vol. 23, no. 3, pp. 383–390, 2022.